RSC Advances

PAPER

View Article Online
View Journal | View Issue

Cite this: *RSC Adv.*, 2025, **15**, 15879

Micellization behavior of an imidazolium surface-active ionic liquid within aqueous solutions of deep eutectic solvents: a comparative spectroscopic study†

Manoj Kumar Banjare, *[a] Kamalakanta Behera,*[b] Malik Abdul Rub[c] and Kallol Kumar Ghosh *[d]

Ionic liquids and deep eutectic solvents are topics of immense importance and are attracting many researchers worldwide owing to their green nature and broader application potential. These green solvents have been widely used in synthesis, catalysis and biocatalysis, nanoscience, pharmaceutics, *etc.* Hence, it is exciting to see how ionic liquids behave within deep eutectic solvents. Here, we examined the aggregation behavior of an imidazolium-based surface-active ionic liquid (SAIL), 1-decyl-3-methylimidazolium tetrafluoroborate [Dmim][BF_4], within aqueous solution of 5 wt% DES choline-based deep eutectic solvents (DESs). Two choline-based DESs (ChCl–urea and ChCl–Gly) were prepared by heating a mixture of 1 : 2 molar ratios of an ammonium salt (choline chloride) with hydrogen bond donors (urea and glycerol). The DESs were characterized using FTIR and ^{1}H-NMR spectroscopic techniques. Micellization behavior of the SAIL [Dmim][BF_4] within these aqueous DESs media was investigated using fluorescence, FTIR, dynamic light scattering (DLS), ^{1}H-NMR, and NOESY. The information about the local microenvironment surrounding the probe molecules and size of the aggregates of [Dmim][BF_4] in the presence of 5 wt% of aqueous DESs were obtained from fluorescence and DLS, respectively. DLS results showed that IL [Dmim][BF_4] forms relatively larger micelles within aqueous solutions of DES ChCl–urea (avg. hydrodynamic radii = 94.6 nm) compared with ChCl–Gly (avg. hydrodynamic radii = 82.8 nm). A significant decrease in the critical micellar concentration and an increase in aggregation number (N_{agg}) were observed, clearly indicating that micellization of IL [Dmim][BF_4] is greatly favored in the DES solutions. FTIR study depicts the strength of intermolecular interactions such as hydrogen bonding, ion–ion pair interactions, and dipole–dipole interactions between the ILs and DESs. The ^{1}H-NMR data showed that differences in chemical shifts can provide significant indication about the IL–DES interactions. ^{1}H-NMR and 1H–1H 2D NOESY spectroscopy were employed to gain insights into these IL–DES interactions that are responsible for the aggregation behavior of the IL [Dmim][BF_4] within aqueous DES solutions. It was observed that IL [Dmim][BF_4] forms self-assembled structures within the aqueous DESs media. The current results are expected to be useful for colloidal aspects of ILs and DESs and their mixtures with water.

Received 18th March 2025
Accepted 24th April 2025

DOI: 10.1039/d5ra01940k

rsc.li/rsc-advances

1. Introduction

A crucial factor in colloidal and surface chemistry is the critical micelle concentration (CMC), which refers to the concentration of ionic liquids (ILs) at which micelles begin to form.[1] Tensiometry, conductometry, calorimetry, and viscometry are a few of the techniques used to calculate CMC.[2–5] It is well known whether they have advantages or drawbacks. Additionally, certain indirect techniques have been utilized by observing the fluorescence of specific probe molecules,[6] with pyrene being a popular choice for the fluorescent probe molecule.[7] ILs are distinctive in their physical and chemical aspects and have a promising future in several industries.[8] Due to their ability to

[a]*Chemistry Division, State Forensic Science Laboratory, Raipur, C.G., 492009, India. E-mail: manojbanjare7@gmail.com; manojbanjarechem111@gmail.com*

[b]*Department of Chemistry, University of Allahabad, Prayagraj, Uttar Pradesh 211002, India*

[c]*Center of Excellence for Advanced Materials Research, King Abdulaziz University, Jeddah-21589, Saudi Arabia*

[d]*School of Studies in Chemistry, Pt. Ravishankar Shukla University, Raipur, C.G. 492010, India*

† Electronic supplementary information (ESI) available. See DOI: https://doi.org/10.1039/d5ra01940k

self-assemble, surface active ILs are exploited as innovative surfactants or designer green solvents.[9] It is remarkable to see that the ILs can create micellar nano-aggregates in aqueous solutions and have capabilities that are similar to those of surface-active agents. ILs show notable physicochemical properties, *i.e.*, high electrical conductivity, high thermal stability, low melting points, low vapor pressure.[10]

Deep eutectic solvents (DESs) are emerging as a new kind of environmentally friendly solvent and analog of ILs.[11] A "deep eutectic solvent (DES)" is a mixture of hydrogen bond donors (HBD) and acceptors (HBA) that creates a eutectic, with a eutectic point temperature lower than that of the melting point of the individual components from which the DES is formed.[12] In traditional DESs, an HBA, such as a quaternary salt, is combined with an HBD, such as amines, carboxylic acids, alcohol, and carbohydrates, in a binary mixture (1 : 1 and 1 : 2 ratio).[13] Due to its low cost, non-toxicity, biodegradability, and economical manufacturing, quaternary ammonium salts—in particular, choline chloride, [Ch]Cl—are the HBA most frequently utilized in DES formulations. This organic substance is generated in large quantities and added to chicken products to boost their growth.[14] Green solvents with a variety of uses have been suggested for DES produced by [Ch]Cl.[15,16] Characteristics of DESs are their low cost, lower toxicity, higher conductivity, relatively lower viscosity, non-flammability, and biodegradability.[17–20] The classification of salt solutions as DESs or any other kind of hydrogen bonding compound in liquid solvents at room temperature, such as water, alcohols, ethylene glycol, glycerine, and so on, is debatable.[21] However, it might be tempting to use the recently proposed definition of DES for aqueous solutions for salts or other compounds.[22]

It is interesting to note that H-bonding essentially controls component interactions, which makes DESs very water-compatible.[23] The combination of DESs' high performance and green/biocompatible features has led to the widespread application of DESs aqueous solutions in many fields. Numerous investigations on reline (the most popular DES, which is made up of urea (U) and choline chloride (ChCl) in a 2 : 1 molar ratio) aqueous dilutions documented the change from a "water-in-DES" system to a "DES-in-water" system at a specific dilution range.[24,25] Numerous basic research has been conducted on "water-in-DES" systems, but "DES-in-water" systems are essentially of little interest (*i.e.*, the system becomes a simple aqueous solution of the constituent components after the breaking of H-bonded complexes).[16,26]

The changes in the micellar properties of surface active ILs within DESs is currently a topic of immense importance owing to the wide-spread application potential of both these green solvents. Hence it is noteworthy to study the IL–DES interactions responsible for the formation of micelles *i.e.*, van der Waals, hydrophobic and electrostatic interactions which contributes to the overall micellization process. The DES is associated with the IL micelles, thereby reducing the CMC of the micelles. The addition of DESs in IL aqueous solutions readily reduces the CMC and micellization behavior is more rapid which is characterized by using different techniques such as fluorescence, UV-visible, FTIR and NMR measurements.

Pandey *et al.*[27] investigated the effects of DESs on the aggregation behavior of various surfactants, *i.e.*, anionic dodecyl sulfate (SDS), cationic dodecyl trimethylammonium bromide (DTAB), zwitterionic dodecyl sulfobetaine (SB-12), and nonionic Triton X-100 (TX-100) in aqueous solutions. It has been observed that the presence of DESs causes a significant change in an aqueous micellar solution's characteristics. Arnold *et al.*'s[28] investigation of sodium dodecyl sulfate (SDS) with deep eutectic solvents (DES) revealed self-assembly formation that was observed by X-ray reflectivity (XRR) and small angle neutron scattering (SANS). SANS data imply that the micelles generated in DES do not have the same shape and size as that observed in water and this work supports the determination of the critical micelle concentration using surface-tension measurements. Zhang *et al.*[29] investigated the aggregation of 1-alkyl-3-methylimidazolium chloride in a 1 : 2 mole ratio of glycerol and choline chloride based deep eutectic solvent. The crucial micellar concentration, micellar size, and intermolecular interactions in IL/DES solutions were examined using the fluorescent probe method, small-angle X-ray scattering, and FTIR spectroscopy. IL CnmimCl micellizes primarily as a result of the solvophobic effect in DES, and the intermolecular hydrogen-bond interaction helps to favor micelle formation.

For the first time, we investigated the self-aggregation behavior of an IL 1-decyl-3-methylimidazolium tetrafluoroborate [Dmim][BF_4] in aqueous solutions of the deep eutectic solvents ChCl–urea and ChCl–Gly, respectively. The aggregation behavior of IL [Dmim][BF_4] within the aforementioned two DES solutions is thoroughly compared utilizing FTIR and ^{1}H-NMR/NOESY spectroscopic techniques. The aggregation behavior of ILs in DESs media would enhance the utility of these green designer solvents and they would also make it easier to develop new solvent systems as self-assembly media in the future.

2. Experimental section

2.1. Materials

The IL used in the study is 1-decyl-3-methylimidazolium tetrafluoroborate [DmimBF_4] (≥99%). Urea (≥99%), potassium bromide (FTIR grade ≥ 99% trace metals basis), potassium chloride (≥99%), choline chloride (≥99%), glycerol (≥99%), pyrene (≥99%), 1-pyrene carboxaldehyde (≥99%) and cetylpyridinium chloride (≥99%) were purchased from Sigma Aldrich Pvt. Ltd with high purity. Deuterium oxides (99.9% for NMR spectroscopy grade) were obtained from Merck KGaA, 64271 Darmstadt, Germany. All the aqueous solutions were prepared using Millipore water. The molecular structure of IL 1-decyl-3-methylimidazolium tetrafluoroborate, urea, and glycerol are represented in Scheme 1.

2.2. Methods

Several techniques such as fluorescence (pyrene and PyCHO used as probes), DLS, FT-IR, and a Bruker NMR spectrometer (using deuterium oxide (D_2O) as a reference solution of NMR)

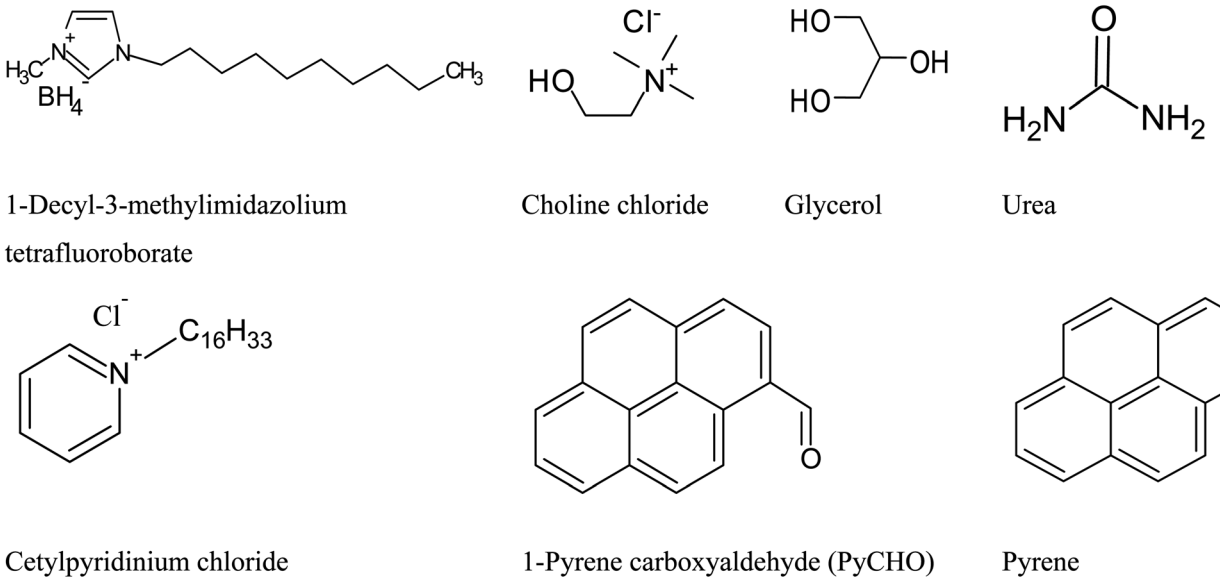

Scheme 1 Structures of IL 1-decyl-3-methylimidazolium tetrafluoroborate, choline chloride, glycerol, urea, cetylpyridinium chloride, pyrene and 1-pyrene carboxyaldehyde.

are used to characterize the synthesized DESs, IL and micellization behavior of ionic liquid within DESs media.

2.2.1 Fluorescence. Fluorescence intensity measurements of pyrene (1.2×10^{-4})/PyCHO (1.2×10^{-4}) in aqueous [DmimBF$_4$] IL (0.01 M) solution in the presence of DESs were performed using a Cary Eclipse fluorescence spectrophotometer (Agilent Technology 679 Springvale Rd, Mulgrave, Victoria, and Australia) and an intense Xenon flash lamp as the light source. All intensity measurements were made at a wavelength of 334 nm for excitation, and a slit width of 5 nm was used to record the emission spectra. An electro-thermally controlled multi-cell holder with a Peltier was used to hold a quartz cuvette containing the sample.[27,29]

2.2.2 Dynamic light scattering (DLS). DLS was used to obtain the [DmimBF$_4$] IL(0.01 M) aggregate size within aqueous DESs media. A Malvern Nano Zetasizer 90 (Malvern apparatus, Japan) apparatus with a He–Ne laser was used to conduct the DLS measurements. All measurements were made at a 90° scattering angle. The micellar solutions were made clean through 0.2 μm needle filters. Solutions of various IL–DESs contents were created to determine the size of the aggregates. The quartz cell was meticulously cleaned with deionized water four–five times before being cut to size. The measurements were done in a temperature-neutral environment.[27,30]

2.2.3 FTIR. FTIR (Model: Nicolet iS10, Thermo Fisher Scientific Instrument, Madison, USA) was used to measure the FT-IR spectra of [DmimBF$_4$] IL, synthesized DESs and aqueous [DmimBF$_4$]–DESs mixtures. The FTIR spectra were captured using a DTGS (deuterated triglycine sulfate) detector with a resolution of 4 cm^{-1} and 32 scans. Each sample underwent at least five different measurements.[28,30]

2.2.4 NMR. Bruker NMR spectrometers running at 400 MHz and using D_2O as the solvent were used to produce the ^{1}H-NMR/NOESY spectra of IL in the presence and absence of DESs. The IL solutions were transferred to 2.5 mm capillary NMR tubes and dried for 48 h at a vacuum pressure of 10^{-2} torr within an argon glove box. After being removed from the glove box, the NMR capillary tubes were first sealed with beeswax and then flame-sealed. To create a deuterium lock signal for the ^{1}H-NMR and 2D-NOESY studies, the sealed 2.5 mm capillary tubes containing the samples were put inside a 5 mm outer diameter NMR tube containing 99.9% D_2O solvent. The ^{1}H-NMR spectra for solutions containing imidazolium cations exhibit a water peak at 2.73 ppm before drying the ILs. Ferreira *et al.*[13] synthesized the ChCl : Gly (1 : 2) based DES and characterized it by NMR.

2.2.5 Preparation of [DmimBF$_4$]/DESs solution. To investigate the micellization properties of [Dmim][BF$_4$], 0.01 M stock solution was prepared in 100 mL of Millipore water. The glycerol and urea based DES was diluted to 5 wt% in 100 mL of Millipore water. Fluorescence intensity measurements included 50 mL of pyrene (1.2×10^{-4} M), or PyCHO (1.2×10^{-4} M) with 50 mL of cetylpyridinium chloride (1×10^{-3}) used as quencher in aqueous solution.

The desired amounts of [DmimBF$_4$]/and glycerine/urea DES were mixed in a sealed bottle. Then, the mixture was stirred until a homogenous solution was formed and characterized by FTIR and NMR techniques as shown in Fig. 1 and 2.

2.3. Preparation of choline based DESs

Choline chloride with glycerol and urea were mixed in the proper molar ratio (1 : 2) and heated at 80 °C until a liquid phase was achieved to create DES. The DES was vacuum-dried for 48 hours at 60 °C before usage. A digital analytical scale (Shimadzu AUX220) was used to precisely measure the weight amounts of water to create the ChCl : Gly (1 : 2) and ChCl : urea (1 : 2) aqueous mixtures (1 to 5 wt%) with an accuracy of ±0.1 mg. By employing an 831 KF coulometer (Metrohm) without

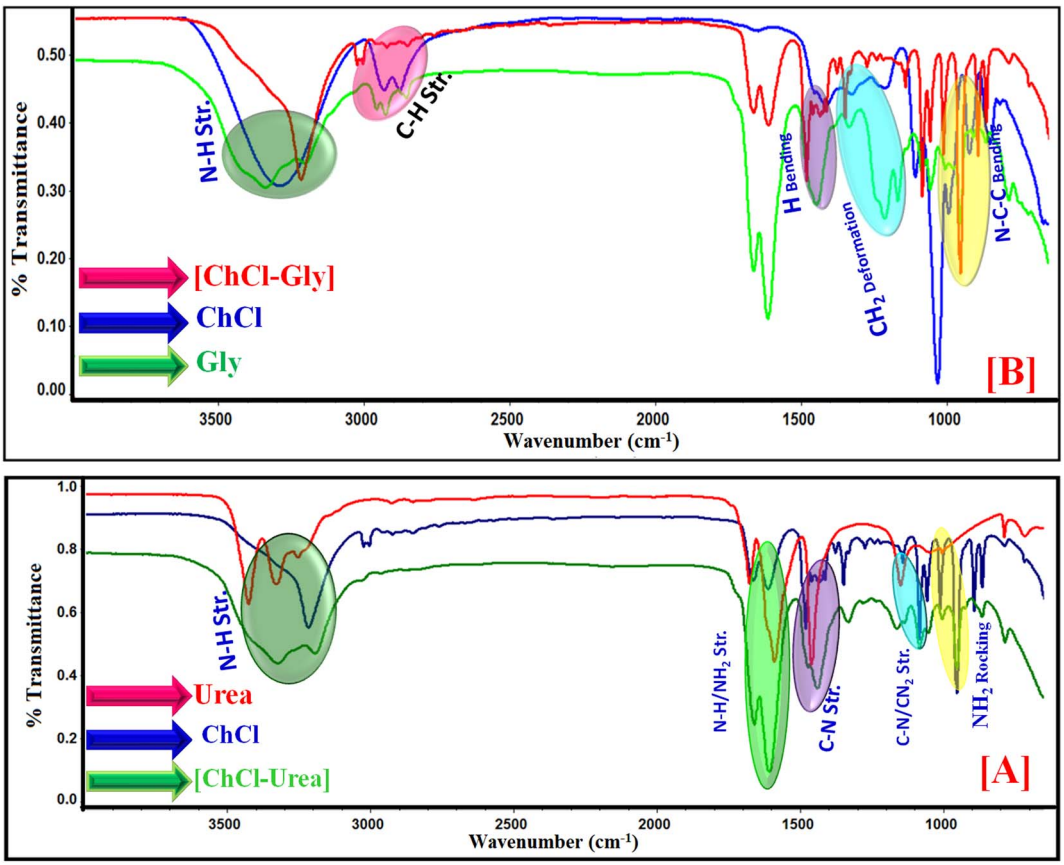

Fig. 1 FT-IR spectra of synthesized ChCl-based DESs: (A) ChCl–urea and (B) ChCl–Gly.

a diaphragm and Hydranal AG (Honeywell) as an analyte, the final water content was verified by Karl Fischer titration.[13]

3. Results and discussion

3.1. Characterization of synthesized choline based DESs

The characterization of synthesized choline based DESs was done by using simple and advanced spectroscopic methods such as FTIR and ^{1}H-NMR. FTIR and ^{1}H-NMR analysis were applied to explore the structure of the deep eutectic solvents made up of choline chloride, urea and glycerol, as shown in Fig. 1.

3.1.1 FTIR study. The interaction between ChCl, urea and Gly was analyzed by FTIR spectroscopy as shown in Fig. 1. The ChCl–urea and ChCl–Gly FTIR spectra are often a combination of frequencies from the ChCl and urea, and Gly FTIR spectra, except for some minor frequency shifts.

The vibrations of the methyl ($-CH_3$) stretching are attributed to the frequencies observed at 3222.21 cm^{-1} in ChCl. The amine ($-NH_2$) symmetric stretching vibration and anti-symmetric stretching vibration are responsible for the frequencies observed at 3428.41 cm^{-1} and 3328.1 cm^{-1} in urea, respectively. The typical vibrational frequency of amide ($-CONH_2$) is observed 1678.50 cm^{-1} and 1592.12 cm^{-1} frequencies.[30,31]

According to this study, the stretching vibration of the O–H functional group may be to point out the glycerol peak values observed at 3320–3345 cm^{-1}. Other significant functional groups show the different IR peaks *i.e.*, (i) asymmetrical-NH_2 stretching at 3417 cm^{-1}, (ii) C–H stretching at 2978 cm^{-1}, (iii) N–H bending at 1730 cm^{-1}, (iv) O–H bending at 1412 cm^{-1}, (v) N–H bend + C–N bending at 1341 cm^{-1}, (vi) CH_2 deformation at 1296 cm^{-1}, (vii) C–C stretch + other vibrations at 1036 cm^{-1}, (viii) N–C–C bending at 936 cm^{-1}. FT-IR spectra of synthesized ChCl–Gly based DESs are shown in Fig. 1(B) and Table 1.

ChCl–urea-based DES bands were changed to wider bands and shifted to a lower frequency. The results indicate the formation of H-bonds between ChCl and urea as shown in Scheme 2. The existence of H-bonds causes the bond force constants of the original bonds to decrease, which causes the absorption frequency to fall and become broader. The system's hydrogen bonds could take the form –NH···OH–, –NH···NH–, –OH···OH– or –OH···NH–. The DESs of ChCl–urea/ChCl–Gly exist in a liquid form at room temperature, which is explained by the presence of H-bonds, which is confirmed by the FTIR spectra. FTIR spectra of the synthesized ChCl–urea based DESs are shown in Fig. 1(A) and Table 2.

3.1.2 ^{1}H-NMR study. To characterize the molecular interaction between the components of DESs, *i.e.*, urea, glycerol and ChCl, ^{1}H-NMR was employed as a sensitive and advanced approach. Fig. 2 shows precise ^{1}H-NMR spectra for urea/Gly-based DESs systems. Compared with the signals obtained for the ChCl and Gly/urea in the D_2O solution, the observed signals

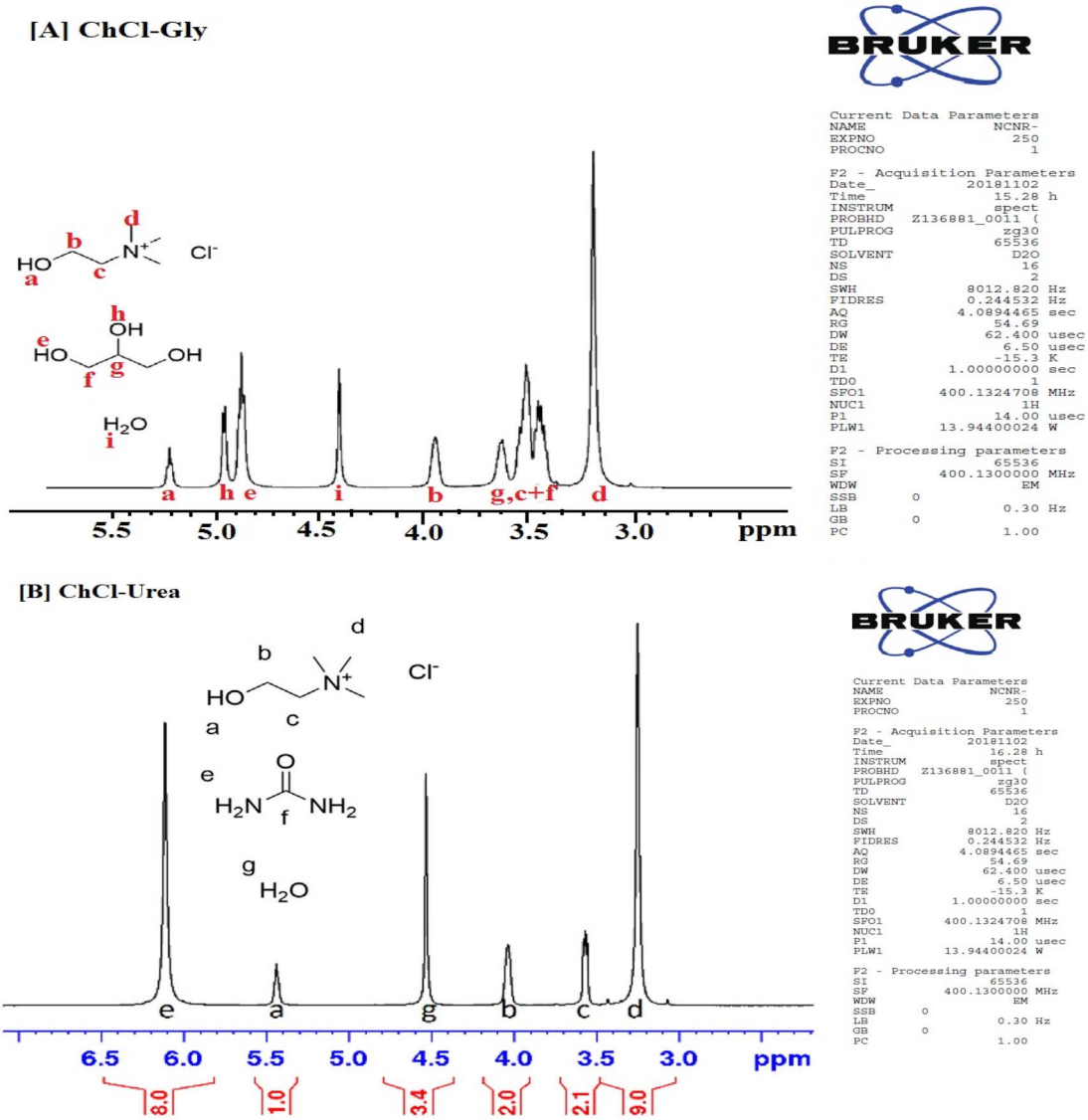

Fig. 2 ^{1}H-NMR spectra of [A] ChCl–Gly- and [B] ChCl–urea-based DESs.

for ChCl and urea/Gly protons in ChCl–urea/ChCl–Gly DESs were shifted downfield (Fig. 2). The downfield chemical shifts confirmed the formation of both DESs as a result of ion-hydrogen bond donor complexes. Results from the ^{1}H-NMR for DESs, urea, and Gly (in D_2O solution) are shown in Fig. 2.[32]

In the current study, the ^{1}H-NMR spectrum (Fig. 2(A)), the signals of the $-CH_3$ group bound to the choline nitrogen, CH_2–N+ (c), and those of two hydroxyl methylenes of glycerol (f), are overlapping; the remainder are perfectly separated: $\delta = 5.08$ (t, $J = 4.7$ Hz, 1H, Ha), 4.82 (d, $J = 4.8$ Hz, 2H, Hh), 4.73 (t, $J = 5.0$ Hz,

Table 1 Comparison of the frequencies of the bands observed in FTIR spectra of ChCl, glycerol and DESs

Assignments	ChCl (cm^{-1})	Gly (cm^{-1})	ChCl–glycerol DES (cm^{-1})
$\nu(NH_2)$ asymmetrical stretching	3417	3410	3339
ν(C–H) stretching	2978	2932	2965
ν(C=O) stretching	1730	1730	1750
ν(N–H + C–N) bending	1341	1345	1335
$\nu(CH_2)$ deformation	1296	1213	1218
ν(C–C) stretching	1036	1034	1057
ν(N–C–C) bending	936	328	956

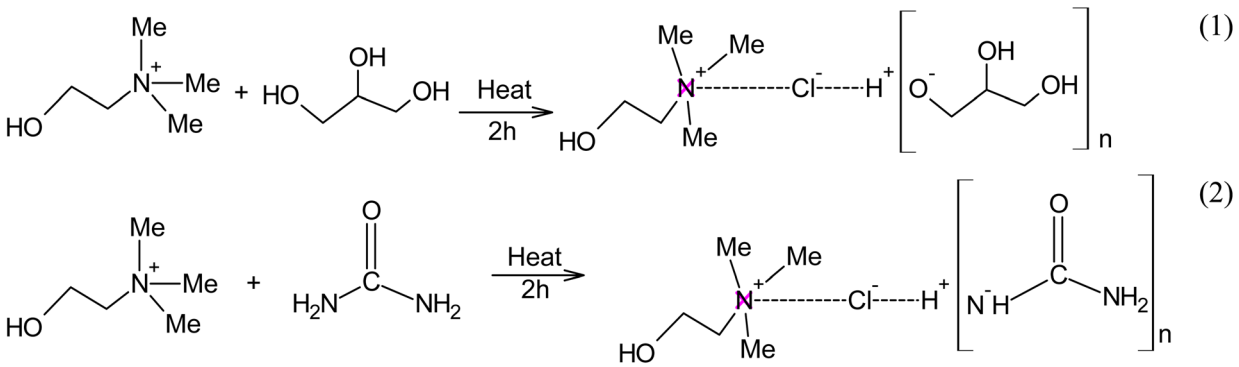

Scheme 2 Synthesis diagram of DESs based on glycerol, urea and choline chloride.

4H, He), 4.26 (s, 2.0H, Hi), 3.76–3.85 (m, 2H, Hb), 3.44–3.53 (m, 2H, Hg), 3.33–3.43 (m, 6H, Hf′, Hc), 3.23–3.33 (m, 4H, Hf), 3.04 (s, 9H, Hd).

All signals of the ^{1}H NMR spectra (Fig. 2(B)) were assigned. For ^{1}H NMR at 298 K, the chemical shifts were: δ 4.04 (s, 2H, Hb), 3.25 (s, 9H, Hd), 4.53 (s, 3H, Hf), 5.40–5.48 (m, 1H, Ha), 3.53–3.60 (m, 2H, Hc), 6.12 (s, 8H, He).

Here, we looked at how the aggregation behavior of long chain-based IL was affected by DESs. To comprehend the chemical process underlying the interaction between the IL and DESs, we used fluorescence spectroscopy, DLS, FT-IR spectroscopy, ^{1}H-NMR and NOESY.

3.2. Determining the CMC of long-chain imidazolium-based IL [DmimBF$_4$] in the presence of DESs using the fluorescence method

This work determined the CMC for the long-chain imidazolium-based IL [DmimBF$_4$]. Following this process, the CMC values for [DmimBF$_4$] were studied in the presence and absence of two choline based DESs: ChCl–urea/ChCl–Gly in aqueous medium.

3.2.1 Pyrene. The CMC of [DmimBF$_4$] micellar systems is often investigated using pyrene as a probe whose fluorescence intensity is affected by the solvent polarity as shown in Fig. S1.† Surprisingly, there isn't a well-established strategy for obtaining a CMC value from pyrene fluorescence data that can be related to fundamental [DmimBF$_4$] micellar characteristics and compared with findings from other methods. The unique vibronic bands of pyrene may be seen in its fluorescence spectrum, which ranges from 340 to 400 nm.[33] The polarities of the microenvironment have a significant impact on these bands' full and virtual intensities, widths, and placements. Even though pyrene is extremely hydrophobic and barely soluble in pure water, it still exhibits partition equilibrium between the aqueous phase and the micellar pseudo phase with a high but finite partition equilibrium constant. The so-called "py-scale" is characterized by the ratio of the fluorescence intensities of the first and third vibronic bands of pyrene (F_1/F_3 ratio), which rises predictably with increasing polarity of the probe environment. The F_1/F_3 ratio around the CMC decreases sigmoidally when the hydrophobic pyrene moves from the aqueous phase to the polar micellar pseudo phase with increasing [DmimBF$_4$] concentrations. Even if it appears to be very prominent, the sigmoid's center is not the only unusual place that cannot be given directly to the CMC of the solution.

The CMC value from experimental plots can be analyzed using a variety of techniques. The interception of the rapidly changing segment of the curve and the almost parallel lower concentration portion of the curve is one way that was used with the pyrene $F_1 : F_3$ approach.[3] The growing sigmoidal curve seen with pyrene fluorescence intensity can be used to determine the CMC (Fig. 3). The concentration of DESs affects the concentration at which IL [DmimBF$_4$] form micelles. The amount of [DmimBF$_4$] affects the fluorescence behavior of the pyrene probe within DESs media and consequently, the CMC, as seen in Fig. 3. In the presence of [DmimBF$_4$], the split significantly increases, indicating the development of micelles at lower concentrations.

3.2.2 PyCHO. The fluorescence behavior of PyCHO within micellar media can be utilized to gain information about the

Table 2 Comparison of the frequencies of the bands observed in the FTIR spectra of ChCl, urea and DES

Assignments	ChCl (cm^{-1})	Urea (cm^{-1})	ChCl–urea DES (cm^{-1})
ν(N–H) in phase	3317	3328	3328
ν(CO)	1686	1667	1664
ν(N–H), ν(NH$_2$)	1629	1592	1611
ν(C–N), ν(CN$_2$) asymmetric	1464	1466	1441
ν(NH$_2$) rocking	1150	1154	1171
ν(C–N), ν(CN$_2$) symmetric stretching	1000	1001	1084
ν(CO), (NH$_2$ + CO)	786	789	959

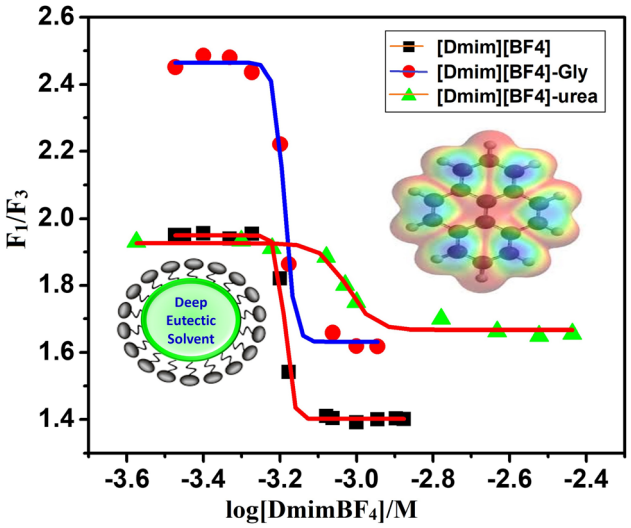

Fig. 3 Graph plot between F_1/F_3 intensity ratios *versus* log[DmimBF$_4$] within the two deep eutectic solvents (water, ChCl–Gly and ChCl–urea, 5 wt%) in aqueous medium at ambient conditions. The lines indicate sigmoidal fitting of the experimental data.

formation of micelles and hence CMC. PyCHO has been seen to be utilized as a fluorescence probe in photo physical analysis of mixed micelles to reveal IL–IL synergistic interactions and the formation of more stable mixed micelles of IL and DESs. Fig. S2† shows the fluorescence spectra of PyCHO in water, and a combination of DESs and water at various compositions. The bands of the PyCHO fluorescence spectrum are clearly defined. The transition of the primary pyrene chromophore is represented by a strong collection of bands between 300 and 400 nm. After the introduction of the –CHO group as a substituent, the general composition of the pyrene absorption spectra remains the same, indicating only minor differences in the probability of alteration between the two molecules. Fluorescence excitation spectra with maximum values similar to 368 nm are caused by the permitted π–π* transition. Fluorophore excitation at 368 nm results in emission spectra with a wavelength maximum at 474 nm. Like other pyrene substituents, the fluorescence maxima exhibit a bathochromic shift with increasing solvent polarity. When IL is consistently added to an aqueous PyCHO solution, the fluorescence intensity first rises and then falls with a hypochromic shift. For IL/DESs mixed systems, some novel findings have also been observed in Fig. 4.[32,34]

PyCHO fluorescence intensity in aqueous and DESs solutions is shown in Fig. 4(A) as a function of [DmimBF$_4$] concentration. Fluorescence intensity substantially decreases following micelle formation as expected when the probe molecules enter the micellar phase, where they encounter an increased hydrophobic microenvironment. The [DmimBF$_4$] CMC values were determined to be 0.9 mM. The CMC values were evaluated from the intensity *versus* concentration [DmimBF$_4$] graph. The relation between fluorescence intensity and [DmimBF$_4$] concentration (mM) is shown in Fig. 4. When micelles started to form, the intensity curve sharply reduced. The computed CMC values for the [DmimBF$_4$] systems were found to be greater in water compared with that of 5 wt% solutions of aqueous DESs. Compared with [DmimBF$_4$]–DESs and [DmimBF$_4$]–H_2O, DESs exhibit notable interactions with the [DmimBF$_4$] system, resulting in a significant reduction in the CMC. The computed CMC values obtained by the fluorescence method using pyrene as the probe is in good agreement. It is important to note that the presence of DESs substantially favors [DmimBF$_4$] micellization.

3.3. Determination of the aggregation number of IL [DmimBF$_4$] micelles in the presence of DESs

Utilizing the steady-state fluorescence quenching approach, we have been able to study the aggregation number (N_{agg}) of micelles. The fluorescence intensity significantly decreased with increasing concentrations of the cetylpyridinium chloride (CPC) quencher for a constant concentration of the long-chain imidazolium-based ionic liquid [DmimBF$_4$] as shown in Fig. S3.† The expression links the micellar concentration [M] to the assumed ratio of fluorescence intensity in the presence and absence of CPC quencher (F) to that in the absence of quencher (F_0):[31]

$$\left(\frac{F}{F_0}\right) = \exp\left(-\frac{[Q]}{[M]}\right) \quad (1)$$

Based on the pseudo-phase representation, the useful micellar concentrations are

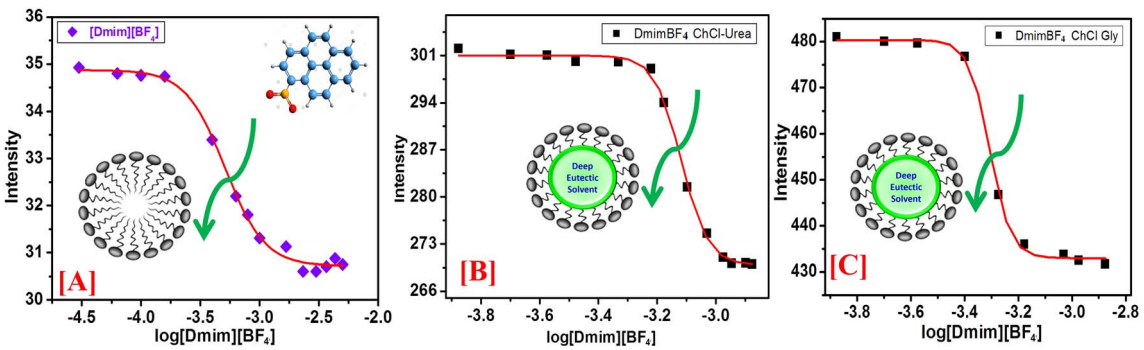

Fig. 4 Plot of PyCHO intensity *versus* log[DmimBF$_4$] (M) concentration within 5 wt% aqueous DESs solution [A] native DmimBF$_4$, [B] DmimBF$_4$–ChCl–urea, [C] DmimBF$_4$–ChCl–Gly. The lines indicate sigmoidal fitting of the experimental data.

$$[M] = \frac{[S] - \text{free monomer}}{N} \quad (2)$$

where $[S]$ is the stoichiometric concentration of the surfactant. The N_{agg} was predicted using the Turro–Yekta relations:[35]

$$\ln\left(\frac{F_0}{F_Q}\right) = \frac{[Q]_{micelle}}{[micelle]} = \frac{[CPC]_{micelle}}{[micelle]_{[DmimBF_4]}} = [CPC]_{micelle}\left[\frac{N_{agg}}{[DmimBF_4] - [CMC]_{[DmimBF_4]}}\right] \quad (3)$$

where F_0 and F_Q represent the intensity of the pyrene fluorescence emission spectrum in the absence and presence of CPC quencher, respectively. The quencher and IL concentrations are $[CPC]_{micelle}$ and $[DmimBF_4]$, respectively. For $[DmimBF_4]$, Fig. 5 shows a profile of $\ln(F_0/F_Q)$ *vs.* [CPC] in aqueous solution. The slopes of these linear profiles are used to calculate the N_{agg} values for the $[DmimBF_4]$–DESs mixed systems and $[DmimBF_4]$ in water, and these values are given in Table 3. Fig. S3† shows that the intensity of fluorescence spectra was decreases as the concentration of [CPC] increases. This clearly suggests that the growth of aggregates is caused by the addition of $[DmimBF_4]$.[34] The values of N_{agg} observed for $[DmimBF_4]$ in a pure aqueous solution are in reasonable accord with those discovered by other literature.[34] In the current study, we found that the value of N_{agg} rises as the CMC value decreases, which is well-documented in a variety of literature data where N_{agg} and CMC values exhibit an opposing tendency. Table 3 makes it quite evident that the CMC of $[DmimBF_4]$ falls upon the inclusion of DESs, while the aggregation number rises. The hydrophobic contacts of DESs with $[DmimBF_4]$ monomers are to blame for these increases in N_{agg}, since they only allow a very small number of IL molecules to gather for the formation of the self-assembled structures. Our aggregate number and CMC results for all the systems under study are very cohesive with one another, whether DESs are present or absent.

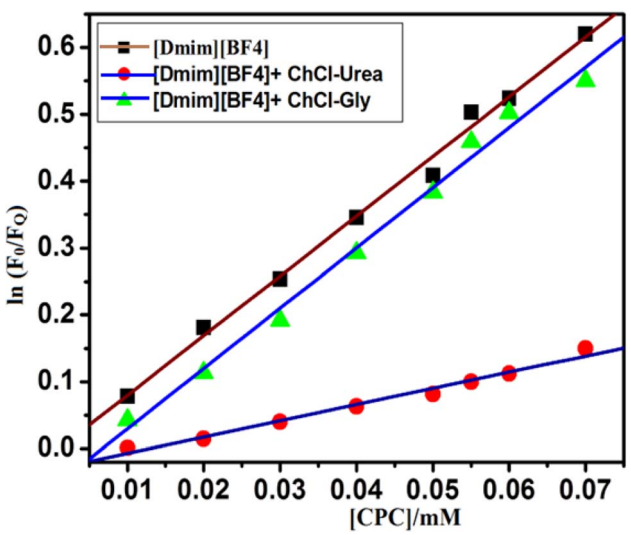

Fig. 5 Plot of $\ln(F_0/F_Q)$ *versus* concentration of CPC (mM) in aqueous $[DmimBF_4]$ (0.01 M) IL solution in the presence of different DESs (5 wt%) at ambient conditions. The lines indicate linear fitting of the experimental data.

Table 3 The CMC, aggregation number (N_{agg}), Stern–Volmer constants (K_{sv}), hydrodynamic radii (Rh) and polydispersity index (PDI) of IL 1-decyl-3-methylimidazolium tetrafluoroborate $[DmimBF_4]$ in the presence and absence of 5 wt% choline based deep eutectic solvents in aqueous solution by the fluorescence method

	CMC (mM)					
DES	Pyrene	1-PyCHO	N_{agg}	K_{sv}	Rh (d nm)	PDI
Water	1.10[a]	1.0	19[a]	10.604[a]	345.3, 55.91[a]	0.698
ChCl–Gly	0.60	0.66	835	10.679	82.8, 17.2	0.820
ChCl–urea	0.53	0.55	225	2.861	94.6, 5.4	0.946

[a] Ref. 34.

3.4. Studying the size distribution of IL $[DmimBF_4]$ micelles by the DLS method

A sensitive method to confirm the nature of the size distribution of tiny particles in a colloidal solution is dynamic light scattering (DLS). The intensity auto-correlation purpose is typically used to study the scope of DLS measurements.[36] Latex size, protein size, nanogold size, and colloid size are the key dimensions that is typically used by DLS. The technique can be used to measure particles with diameters as small as a nanometer; however, it works best for submicron particles. Additionally, DLS can be utilized to examine complex liquids including micelles and microemulsions.

3.4.1 Determining the size distribution of IL $[DmimBF_4]$ micelles. DLS was applied to obtain information about the formation of micelle like aggregates by IL $[DmimBF_4]$ within aqueous DESs solutions. The concentrations of the pure imidazolium-based IL $[DmimBF_4]$ were maintained higher than CMC values. The average size of micellar aggregates in 0.01 M $[DmimBF_4]$ solution in the presence of urea/Gly based DESs was measured using DLS. When ChCl–urea and ChCl–Gly-based DESs were added, the scattering intensity *versus* diameter (D) was evaluated at room temperature. $[DmimBF_4]$ IL aqueous solution has a bimodal distribution. The DLS findings (Table 3) clearly show that the peak width of micellar aggregates is comparable for both DESs.

3.4.2 Size distribution of IL $[DmimBF_4]$ micelles in the presence of DESs. Through the DLS study with 5 wt% choline based DESs and $[DmimBF_4]$ IL in aqueous medium, it has been noticed that the change in the hydrodynamic size of IL aggregates caused by $[DmimBF_4]$–DES interactions is likely. Size distribution curves in Fig. 6 show how the hydrodynamic diameter (Rh) for $[DmimBF_4]$–DESs systems have been modified. These results of differences in hydrodynamic size provide a suggestion of the many complex scenarios created in $[DmimBF_4]$–DESs systems. The Rh value were falls from 345.3, 55.91 nm (ref. 34) to 82.8, 17.2 nm as $[DmimBF_4]$ in 5 wt% ChCl–Gly,[30,31,33] as shown in Fig. 6(B). This change in the R_h values can be explained by the fact that smaller aggregates are formed as the electrostatic repulsion between the head groups

decreases *via* IL–DES interactions, allowing [DmimBF$_4$] molecules to move closer to one another and produce compact aggregates. Because of the electrostatic interactions between DESs and [DmimBF$_4$] followed by contraction of the DES backbone, and ChCl–urea was shown in Fig. 6(C). However, as urea concentration rises, DES produces electrostatic repulsion and steric hindrance on the surface of the aggregates, which causes the large aggregates to break apart and produce smaller aggregates.[31]

The peak then becomes broad and grows in size until it reaches 345.3, 55.91 nm (ref. 34) to 94.6, 5.4 nm with the addition of urea-based DES,[30,31,33] which indicates the formation of [DmimBF$_4$] aggregates with DES. As a result, in the [DmimBF$_4$]–DES mixed systems under study, the solutions experience strong attractive binding that is supportive before and after complete charge neutralization. After complete charge neutralization, electrostatic repulsions play a crucial role. Two detached peaks above [DmimBF$_4$] have been seen together with drops in the Rh value of the [DmimBF$_4$]–Gly complexes suggesting strong IL–DES interactions. Before adding ChCl-based DESs, several different parameters can affect the micellar structure of the imidazolium-based IL [DmimBF$_4$].

Electrostatic interactions, hydrophobic interaction, and water structures make up these components. The unpleasant repulsive force between the head groups of the [DmimBF$_4$] IL can be lessened by the BF_4^- ion from the IL. This increases the likelihood that the IL molecules will coalesce more tightly and form bigger aggregates.

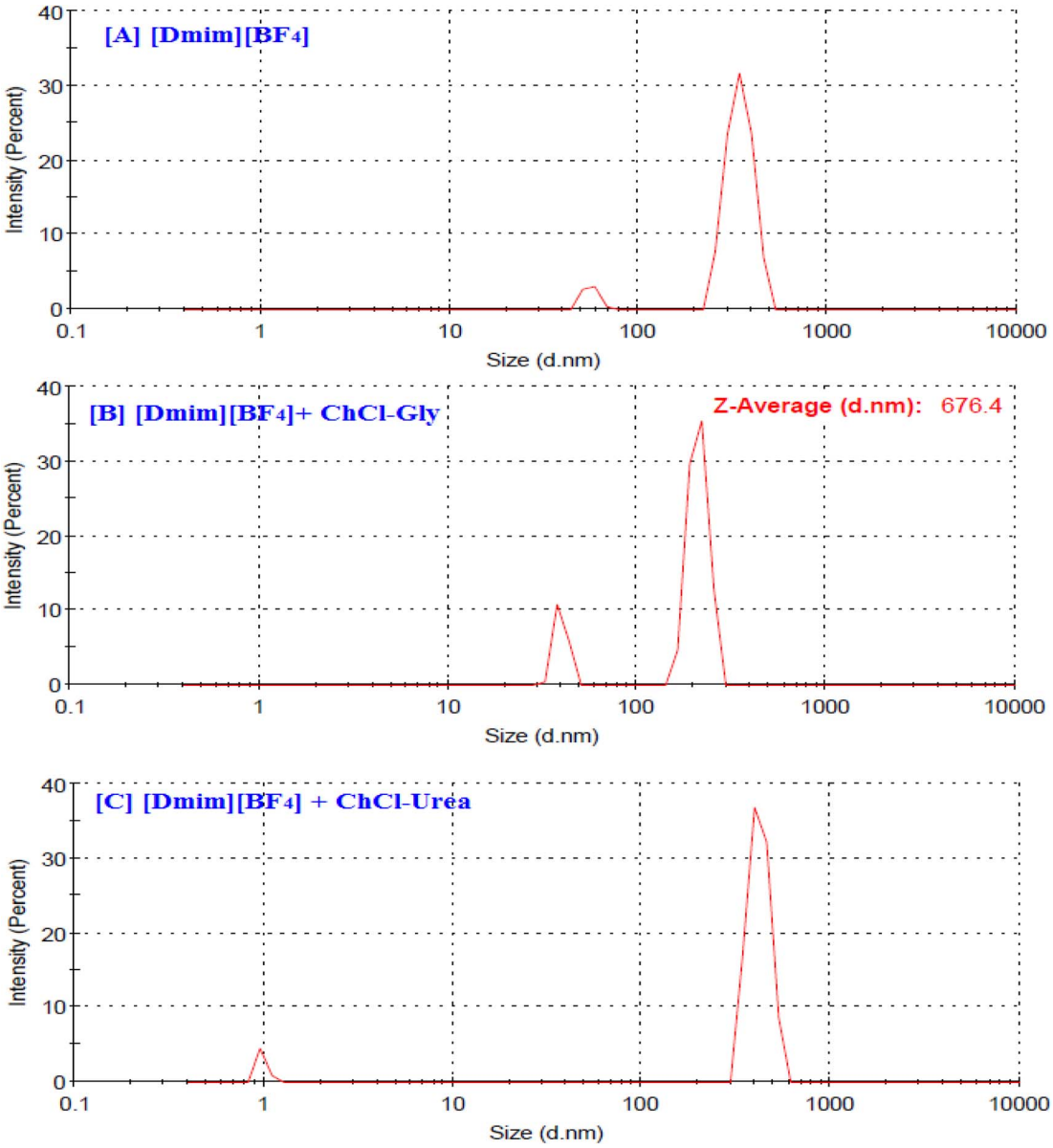

Fig. 6 Size distribution obtained from DLS for aqueous [Dmim][BF$_4$] in the presence and absence of deep eutectic solvents *i.e.*, [A] pure [DmimBF$_4$] in water; (B) [DmimBF$_4$] in ChCl–Gly aqueous solution; and (C) [DmimBF$_4$] in ChCl–urea aqueous solution.

3.5. FTIR spectral response of imidazolium-based ionic liquid [DmimBF$_4$] in the presence of DESs

FTIR spectroscopy is an appealing technique for determining the type of interactions in micellar solutions. A variety of modifications occur in the DESs' mechanism during the amalgamation process. The molecular structure of urea, glycerol, choline chloride, and ionic liquid can be assessed analytically using FTIR spectroscopy. The ions that make up the materials' intra-molecular vibrational modes are frequently extremely sensitive to their local potential energy environment. The self-aggregation of DESs and [Dmim][BF$_4$] in aqueous solution *via* hydrogen bond interactions in the current study results in an IR spectral shift.[37] Fig. S4† and Table 4 depicts the infrared (IR) spectra of the DES–[Dmim][BF$_4$] micellar mixtures.

The deep eutectic solvent of urea is examined using FTIR analysis to determine its microstructure, as illustrated in Fig. 1. To analyze and pinpoint the structures of chemical bonds from the IR frequencies, one can learn about the interactions between various groups through FTIR spectroscopy. The FTIR spectroscopy of ChCl, urea, and Gly is shown in Fig. 1. It should be noted that the IR spectrum of urea is typically the union of the frequencies in the IR spectra of ChCl and urea, with a few frequency shifts.

3.5.1 FT-IR of 1-decyl-3-methylimidazolium tetrafluoroborate with ChCl–Gly. The FT-IR spectra of 1-decyl-3-methylimidazolium tetrafluoroborate within the ChCl–Gly mixture shows that the symmetric and asymmetric stretching CH_2 vibration of alkyl chains observed at 2923.48 cm^{-1} is shifted to 2926.26 cm^{-1}, the aromatic C=C stretching vibration observed at 1574.11 cm^{-1} is shifted to 1655.68 cm^{-1}, the C–N stretching band observed at 1466.68 cm^{-1} is shifted to 147956 cm^{-1}, the C–H in-plane-bending observed at 1170.64 cm^{-1} is shifted to 1083.64 cm^{-1}, the ν[CH$_2$] bending band at 1049.49 cm^{-1} is shifted to 1048.60 cm^{-1}, the aromatic C–H bending observed at 848.21 cm^{-1} is shifted to 955.59 cm^{-1}. The FT-IR spectra of IL [Dmim][BF$_4$] within ChCl–urea DES media is shown in Fig. S4(B).†

3.5.2 Studying the FT-IR of 1-decyl-3-methylimidazolium tetrafluoroborate with ChCl–urea. The FT-IR spectra of 1-decyl-3-methylimidazolium tetrafluoroborate within the ChCl–urea mixture shows that the symmetric and asymmetric stretching CH_2 vibration of alkyl chains at 2923.48 cm^{-1} is shifted to 3021.71 cm^{-1}, the aromatic C=C stretching at 1574.11 cm^{-1} is shifted to 1721.29 cm^{-1}, the C–N stretching band at 1466.68 cm^{-1} is shifted to 1479.61 cm^{-1}, the C–H in-plane-bending at 1170.64 cm^{-1} is shifted to 1083.74 cm^{-1}, ν[CH$_2$] at 1049.49 cm^{-1} is shifted to 1050 cm^{-1}, the aromatic C–H bending observed at 848.21 cm^{-1} is shifted to 954.59 cm^{-1}. FT-IR spectra of IL [Dmim][BF$_4$] within synthesized deep eutectic solvent ChCl–urea media is shown in Fig. S4(C).†

Our findings show how different types of IL–DES interactions *e.g.*, H-bonding and electrostatic interactions play crucial role in the micellization process in aqueous medium. The ChCl–Gly mixture's frequency is less shifted than expected, except for the urea mixture, which was the subject of an additional NMR analysis for confirmation. It is an important means of attributing the interactions in IL and DES solutions.

3.6. ^{1}H-NMR of IL [Dmim][BF$_4$] within DESs

Nuclear magnetic resonance (NMR) spectroscopy is a cutting-edge chemical method used in excellent control and research to assess a sample's purity, molecular structure, and proton position. As an example, NMR allows for the quantitative analysis of mixtures, including recognized and unidentified substances. NMR can also be used in conjunction with spectral analysis to infer the fundamental structure of unknown substances. Once the fundamental structure has been established, NMR can be utilized to analyze physical parameters and confirm molecule conformation in solution.[38]

Proton NMR investigation reveals the effects of DESs on aqueous imidazolium-based IL solutions. NMR is a useful tool for examining how the environment changes during the micellization process. At 298 K, ^{1}H-NMR spectra for 1-decyl-3-methylimidazolium tetrafluoroborate [Dmim][BF$_4$], a long chain imidazolium-based IL, were recorded in the absence and presence of DESs. Because of the ^{1}H-NMR spectrum, it is possible to imagine how the [Dmim][BF$_4$] aggregation behavior and molecular environments are related to the line-shape transform. The chemical shifts (δ) and line widths of IL peaks are sensitively influenced by the composition of the systems, which represents the incidence of change in the IL's local environment, according to a comparison of the ^{1}H NMR spectra of neat [Dmim][BF$_4$] and their mixtures with ChCl–urea and ChCl–Gly.

For ease of assessment, Fig. S5† displays ^{1}H-NMR's confidence in the composition of the IL/DESs mixes under investigation. As previously mentioned, the aromatic protons, whose signals travel upfield in the presence of DESs, exhibit the shifts

Table 4 IR characteristic band of [Dmim][BF$_4$] and mixed [Dmim][BF$_4$]–DESs system

	Wavenumber (cm^{-1})		
Functional groups	[Dmim][BF$_4$]	[Dmim][BF$_4$]–ChCl–Gly	[Dmim][BF$_4$]–ChCl–urea
C–H stretching	2923.48	2926.26	3021.71
ν[CH$_2$] bending	1049.49	1048.60	1050.12
Aromatic C=C stretching	1574.11	1655.68	1721.29
C–N stretching	1466.68	1479.56	1479.61
C–H in-plane-bending	1170.64	1083.64	1083.74
Aromatic C–H bending	848.21	955.59	954.59

for IL that are most sensitive to their presence. Due to the competition between [Dmim][BF_4] and BF_4 for DESs, the ability of the aromatic protons to continue H···BF_4 H-bonds has weakened. This is most apparent for the imidazolium ring's H2, which is primarily acidic. Protons in the methyl (H6) and methylene (H7) groups next to the aromatic ring show negligible modifications. The p–p stack influences these groups' chemical changes as they enter the shielding cones above and below the neighboring rings. In line with theories put forth for similar systems, the chemical shifts of H8 and the terminal methyl protons marginally increase with dilution. This is most likely caused by a partial switch from *gauche* to *trans* conformation. In the current investigation, the imidazolium-based IL concentration was used to compute the proton chemical shifts of [Dmim][BF_4] in D_2O-rich solutions. Table 5 provides direct evidence of [Dmim][BF_4] aggregation in ChCl-based DESs.

Compared with the results obtained for the ChCl and Gly pioneer in the D_2O solution, the characteristic signals of both ChCl and Gly protons in the ChCl–Gly mixture were downfield displaced (Fig. S5†). The creation of an ion-hydrogen bond-donor complex was identified as the key downfield chemical alterations that define DESs. Our findings support the structure of ChCl–Gly DES produced synthetically. All of the holmium ion's protons in ethylene undergo a chemical shift change; however, it is only about half as great as what was seen with urea.[39]

This alteration happens as a result of the differential hydration of the different species that make up DESs, which allows water molecules to enter the preexisting molecular configurations in neat DESs. Increased H-bonding interactions between urea and the water molecules may be the cause of the up-field shift of protons seen in the instance of urea with the addition of water. As a result, the area is contained in the H-bonded urea-water network. Peak broadening and a reduction in spin–lattice relaxation time are the results of such confinement. The relevance of van der Waals interactions between weakly hydrated nanostructured domains of choline ions was also shown to rise with an up-field shift. The aforementioned hypothesis is supported by the absence of cross peaks between protons of the choline ion with either urea or water in urea–water combinations.[40,41]

3.7. 2D-NOESY study of IL with DESs

The possible use of forming a micellar structure using ionic liquids and DES mixtures is demonstrated, along with interpretations of the NMR signals that are relevant to it, such as relaxation periods, chemical shifts, binding constants, NOE factors, self-diffusion coefficients, *etc.*[42] Changes in the molecular structure, which are connected to variations in the defining characteristics of aggregation, have been investigated using proton and NOESY NMR spectroscopy. The obtained NMR spectra are displayed in Fig. S6.† As a result of the water, the addition of both DESs causes a change in the chemical shift of various [Dmim][BF_4] protons. In ^{1}H NMR spectra of urea DES, all four urea protons were present as a singlet. They also exhibit a consistent up-field shift and peak broadening when they transition from clean DES to a DES–water (5% w/w) mixture. Urea's choline ion causes a chemical shift that is visible at the up-filed shift. Compared with other protons, the –CH_3 group exhibits the greatest up-field shift in a mixture of urea and water (5% w/w).

Furthermore, NOESY data clarified that the strength of 1H–1H correlation peaks caused by the interaction of urea and water protons increased with urea/gly water content as shown in Scheme 3 and 4. The structure of the ChCl–Gly-based DES was identified using ^{1}H NMR analysis.

3.7.1 NOESY NMR-based structure calculation. Qualitative analysis of NOESY results was accomplished by a cross-relaxation matrix analysis of [Dmim][BF_4], and ChCl–Gly, ChCl–urea to determine relative 1H locations. It should be pointed out that one must scale NOESY cross-peaks involving more than one hydrogen.[43] Cross-peaks were observed between the H2, H3, and H4 ring proton (Fig. S6†) and the methylene protons H1, the ring methyl protons H1–H5, and the ring proton nearest to the methylene carbons. 2D-NOESY experiments were performed for the system of 0.01 M [Dmim][BF_4] mixed with a 5 wt% solution of DESs. 2D-NOESY experiments give excellent insights into the nature of the self-assembly process in several aggregated systems. The two NMR NOESY spectra are shown in Fig. 9. In both cases, we observe strong cross-peaks between the protons in the head group regions of IL with DESs aggregates. Additional cross-peaks are observed between the terminal methyl group of both cationic surfactants and the *n*-methylene protons of the [Dmim][BF_4] and the head group protons. Indeed, if we examine the aromatic protons at around 7.25–8.25 ppm, we see the existence of cross peaks between the aromatic protons and the first few chain protons in the [Dmim][BF_4]; we clearly observe a cross peak between the aromatic protons (7.25–8.25 ppm) and the OH protons in the DESs molecules. From the NOESY spectra of both DES systems shown here, we observed strong correlations between the a-protons of [Dmim][BF_4] and the head group protons of the DESs (7.3–8.5 ppm). We also observed a strong correlation between the 1H methyl protons of [Dmim][BF_4] with urea (3.989 ppm), Gly (3.971 ppm), and the [Dmim][BF_4] long hydrocarbon chain protons (4.162 ppm). We also see several other correlations in the region around 3.796 ppm; these represent cross-peaks between the *x*-CH_3 peak of [Dmim][BF_4] and the NH_2 protons of urea.

Table 5 Chemical shift values for the protons of [Dmim][BF_4], IL–ChCl–Gly and IL–ChCl–urea

Proton of [Dmim][BF_4]	H1	H2	H3	H4	H5	H6	H7–H13	H14
[Dmim][BF_4] (ppm)	3.796, 3.749, 3.720	8.490	7.376	7.319, 7.307	4.093, 4.023	1.717	1.175, 1.127	0.727, 0.569
[Dmim][BF_4]–ChCl–urea (ppm)	3.989, 3.676, 3.652	8.558	7.451	7.387, 7.334	4.162, 4.078	1.994	1.756, 1.593	0.620, 0.606
[Dmim][BF_4]–ChCl–Gly (ppm)	3.971, 3.965	8.526, 8.498	7.356	7.307	4.047, 4.031	1.967	1.297, 1.200, 1.142	0.737, 0.723

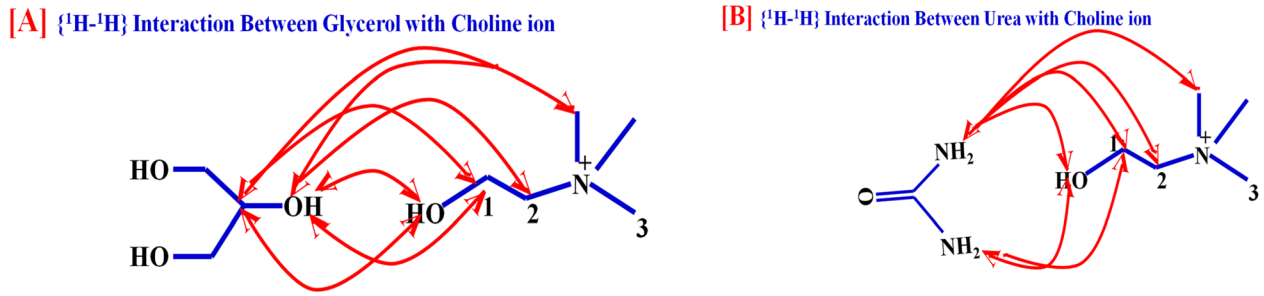

Scheme 3 {1H–1H} interactions of ChCl with glycerol and urea.

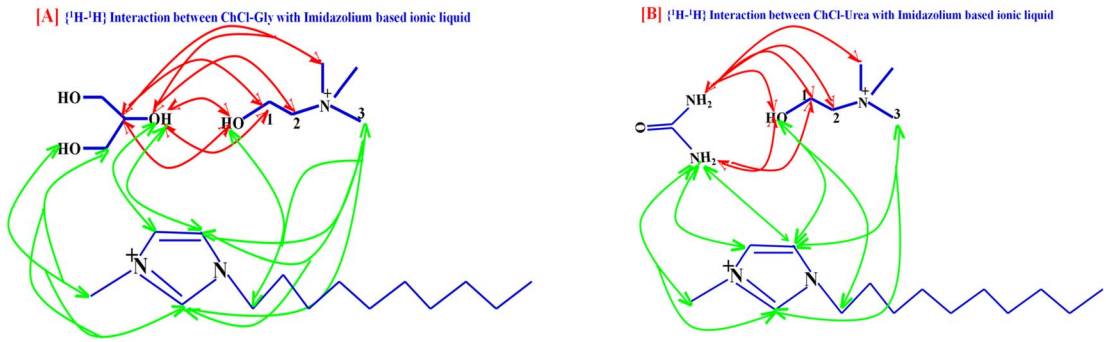

Scheme 4 Schematic representation of the {1H–1H} interactions of the following DESs with [Dmim][BF4]: [A] glycerol and [B] urea.

The complexation of DESs was performed using distance restraints obtained from cross-peaks of a NOESY contour map recorded at 600 MHz. Fig. S6† shows the relative intensities of some of the NOE cross-peaks observed in the 2D-NOESY experiment. Sequential connectivities could be observed through the analysis of NOESY contour maps (Fig. S6†). Despite the good dispersion of amide hydrogen chemical shifts, values from *d* 6.00 ppm to 8.60 ppm can be observed with some signal overlaps attributable based on their connectivity to Gly and urea signals. Additionally, the nuclear Overhauser effect measurement is one of the most important tools to prove the formation of the complexation. The NOESY technique is very useful to gain insights into the geometry of the complex.

The NOESY contour map of the DESs–IL mixture shows some differences compared with the free NMR spectrum. Only sequential and intra-residue cross-peaks were assigned in the contour maps. The NOESY contour map showed the intermolecular NOE correlation between hydrogens H4–DES, H2–DES, H3–H6, and H2–H7/H13.

In general, the head part imidazolium ring of the ionic liquid has more interaction with the –OH/NH_2 group of ChCl/Gly/urea, which is confirmed by 2D-NOESY results, as shown in Fig. S6.† Regarding the interactions among IL protons in the aqueous mixtures, we emphasize that cross-peaks between aliphatic and aromatic protons, as well as between protons in non-neighboring alkyl groups, are visible at all water contents investigated, even the highest, where IL molecules are presumably aggregated in micelle-like structures. Although we cannot draw any definitive conclusion about the organization of the apolar chains from the present observations, it appears that the tails are not fully segregated in hydrophobic domains for both ILs, as expected for spherical aggregates.[44,45] The {1H–1H} interactions of ChCl with glycerol and urea was shown in Scheme 3 and the {1H–1H} interactions of IL with synthesized DESs [A] glycerol and [B] urea were shown in Scheme 4.

4. Conclusions

This manuscript investigates the aggregation behavior of a surface-active ionic liquid (SAIL) within an aqueous solution of deep eutectic solvents (DESs). The choline chloride based DESs ChCl–urea and ChCl–Gly are prepared first and then the micellization behavior of long-chain imidazolium-based IL [Dmim][BF_4] is studied using various spectroscopic techniques such as fluorescence, DLS, FT-IR, ^{1}H-NMR and NOESY. The purpose of the current study was to assess the IL–DES interaction that is responsible in the [Dmim][BF_4] aggregate formation within the aqueous choline-based DESs media. A significant decrease in the CMC values and an increase in N_{agg} in aqueous choline-based DESs solutions indicate an overall favorable micellization process. The CMC value of [Dmim][BF_4] in an aqueous solution of ChCl–Gly DES is observed to be slightly larger than that in ChCl–urea DES solution, which shows the importance of HBD of DES in favoring the micellization of SAIL in the solution. DLS results indicate that the assemblies of SAIL formed in aqueous ChCl–urea are relatively widely distributed compared with ChCl–Gly, while the size distribution of the [Dmim][BF_4] micelles in aqueous solution is narrow. The strength of hydrogen bond interactions between ChCl (HBA) and HBD (glycerol and urea) was investigated from FT-IR

spectral responses. This current study further enhances the potential applications of these green designer solvents as media for a variety of synthesis, catalysis, and biocatalysis reactions.

Conflicts of interest

All authors declare no competing financial interest.

Acknowledgements

The authors are grateful to the National Center for Natural Resources, Pt. Ravishankar Shukla University, Raipur (C.G.), for providing access to the nuclear magnetic resonance instrument and to Prof. S. Saraf, School of Studies in Pharmacy, Pt. Ravishankar Shukla University, Raipur (C.G.), for providing the experimental facilities to measure the aggregate size distribution obtained from dynamic light scattering (DLS). We also acknowledge Prof. M. K. Deb, Head, School of Studies in Chemistry, Pt. Ravishankar Shukla University, Raipur (C.G.), for providing access to the FTIR and laboratory facility. No funding is available in research works.

References

1 A. A. C. Toledo Hijo, E. K. Silva, A. A. D. Meirelles, R. L. Cunha and A. J. A. Meirelles, Novel naturally derived encapsulation agents in the ionic liquid form for sustainable emulsion-based products, *Sustainable Food Technol.*, 2023, **1**, 275–279.

2 E. Gale, R. H. Wirawan, R. L. Silveira, C. S. Pereira, M. A. Johns, M. S. Skaf and J. L. Scott, Directed discovery of greener cosolvents: new cosolvents for use in ionic liquid based organic electrolyte solutions for cellulose dissolution, *ACS Sustainable Chem. Eng.*, 2016, **4**, 6200–6207.

3 J. H. Clark, T. J. Farmer, L. H. Davila and J. Sherwood, Circular economy design considerations for research and process development in the chemical sciences, *Green Chem.*, 2016, **18**, 3914–3934.

4 L. M. Gilbertson, J. B. Zimmerman, D. L. Plata, J. E. Hutchison and P. T. Anastas, Designing nanomaterials to maximize performance and minimize undesirable implications guided by the Principles of Green Chemistry, *Chem. Soc. Rev.*, 2015, **44**, 5758–5777.

5 K. S. Egorova, E. G. Gordeev and V. P. Ananikov, Biological activity of ionic liquids and their application in pharmaceutics and medicine, *Chem. Rev.*, 2017, **117**, 7132–7189.

6 G. García, S. Aparicio, R. Ullah and M. Atilhan, Deep eutectic solvents: physicochemical properties and gas separation applications, *Energy Fuels*, 2015, **29**, 2616–2644.

7 N. Kaur and V. Singh, Current status and future challenges in ionic liquids, functionalized ionic liquids and deep eutectic solvent-mediated synthesis of nanostructured TiO_2: a review, *New J. Chem.*, 2017, **41**, 2844–2868.

8 P. S. Gehlot, A. Kulshrestha, P. Bharmoria, K. Damarla, K. Chokshi and A. Kumar, Surface-active ionic liquid cholinium dodecylbenzenesulfonate: self-assembling behavior and interaction with cellulase, *ACS Omega*, 2017, **2**, 7451–7460.

9 J. Eastoe, S. Nave, A. Downer, A. Paul, A. Rankin and K. Tribe, Adsorption of ionic surfactants at the air-solution interface, *Langmuir*, 2000, **16**, 4511–4518.

10 A. Pyne, J. Kuchlyan, C. Maiti, D. Dhara and N. Sarkar, Cholesterol based surface active ionic liquid that can form microemulsions and spontaneous vesicles, *Langmuir*, 2017, **33**, 5891–5899.

11 E. L. Smith, A. P. Abbott and K. S. Ryder, Deep eutectic solvents (DESs) and their applications, *Chem. Rev.*, 2014, **114**, 11060–11082.

12 M. A. R. Martins, S. P. Pinho and J. A. P. Coutinho, Insights into the nature of eutectic and deep eutectic mixtures, *J. Solution Chem.*, 2018, **48**, 962–982.

13 A. S. D. Ferreira, R. Craveiro, A. R. Duarte, S. Barreiros, E. J. Cabrita and A. Paiva, Effect of water on the structure and dynamics of choline chloride/glycerol eutectic systems, *J. Mol. Liq.*, 2021, **342**, 117463.

14 O. S. Hammond, D. T. Bowron and K. J. Edler, The effect of water upon deep eutectic solvent nanostructure: an unusual transition from ionic mixture to aqueous solution, *Angew. Chem., Int. Ed.*, 2017, **56**(33), 9782–9785.

15 C. Pelosi, J. G. Rivera, M. R. Tiné, G. Ciancaleoni, L. Bernazzani and C. Duce, Evaluation of physicochemical properties of Type-II deep eutectic solvents/Water mixtures based on choline chloride and calcium/magnesium chloride hexahydrate, *J. Mol. Liq.*, 2023, **392**, 123459.

16 N. L. Salas, J. M. V. Luna, S. Imberti, E. Posada, M. J. Roldán, J. A. Anta, S. R. G. Balestra, R. M. M. Castro, S. Calero, R. J. J. Riobóo, M. C. Gutiérrez, M. L. Ferrer and F. D. Monte, Looking at the "water-in-deep-eutectic-solvent" system: a dilution range for high performance eutectics, *ACS Sustainable Chem. Eng.*, 2019, 7(21), 17565–17573.

17 D. Yu, X. Huang, M. Deng, Y. Lin, L. Jiang, J. Huang and Y. Wang, Effects of inorganic and organic salts on aggregation behavior of cationic gemini surfactants, *J. Phys. Chem. B*, 2010, **114**, 14955–14964.

18 J. Bowers, M. J. Danks and D. W. Bruce, Surface and aggregation behavior of aqueous solutions of Ru(II) metallosurfactants: 1. Micellization of [Ru(bipy)(2)(bipy ')][Cl](2) complexes, *Langmuir*, 2003, **19**, 292–298.

19 S. E. Sandler, B. Fellows and O. T. Mefford, Best practices for characterization of magnetic nanoparticles for biomedical applications, *Anal. Chem.*, 2019, **91**(22), 14159–14169.

20 S. P. M. Ventura, F. A. Silva, M. V. Quental, D. Mondal, M. G. Freire and J. A. P. Coutinho, Ionic-liquid-mediated extraction and separation processes for bioactive compounds: past, present, and future trends, *Chem. Rev.*, 2017, **117**, 6984–7052.

21 A. Rehman and X. Zeng, Ionic liquids as green solvents and electrolytes for robust chemical sensor development, *Acc. Chem. Res.*, 2012, **45**, 1667–1677.

22 H. F. Hizaddin, A. Ramalingam, M. A. Hashim and M. K. O. H. Kali, Evaluating the performance of deep eutectic solvents for use in extractive denitrification of

liquid fuels by the conductor-like screening model for real solvents, *J. Chem. Eng. Data*, 2014, **59**, 3470–3487.

23 X. Ge, C. Gu, X. Wang and J. Tu, Deep eutectic solvents (DESs)-derived advanced functional materials for energy and environmental applications: challenges, opportunities, and future vision, *J. Mater. Chem. A*, 2017, **5**, 8209–8229.

24 S. Sarmad, Y. Xie, J. P. Mikkola and X. Ji, Screening of deep eutectic solvents (DESs) as green CO2 sorbents: from solubility to viscosity, *New J. Chem.*, 2017, **41**, 290–301.

25 O. S. Hammond, D. T. Bowron and K. J. Edler, Liquid structure of the choline chloride-urea deep eutectic solvent (Urea) from neutron diffraction and atomistic modeling, *Green Chem.*, 2016, **18**, 2736–2744.

26 R. Stefanovic, M. Ludwig, G. B. Webber, R. Atkin and A. J. Page, Nanostructure, hydrogen bonding and rheology in choline chloride deep eutectic solvents as a function of the hydrogen bond donor, *Phys. Chem. Chem. Phys.*, 2017, **19**, 3297–3306.

27 M. Pal, K. Behera, A. Yadav and S. Pandey, Modifying properties of aqueous micellar solutions by external additives: deep eutectic solvent versus its constituents, *ChemistrySelect*, 2018, **3**, 12652–12660.

28 T. Arnold, A. J. Jackson, A. S. Fernandez, D. Magnone, A. E. Terry and K. J. Edler, Surfactant behavior of sodium dodecylsulfate in deep eutectic, solvent choline chloride/urea, *Langmuir*, 2015, **31**, 12894–12902.

29 X. Tan, J. Zhang, T. Luo, X. Sang, C. Liu, B. Zhang, L. Peng, W. Li and B. Hana, A facile approach to obtain highly tough and stretchable LAPONITE®-based nanocomposite hydrogels, *Soft Matter*, 2016, **12**, 5297–5303.

30 M. K. Banjare, K. Behera, M. L. Satnami, S. Pandey and K. K. Ghosh, Self-assembly of short-chain ionic liquid within deep eutectic solvents, *RSC Adv.*, 2018, **8**, 7969–7979.

31 R. K. Banjare, M. K. Banjare, K. Behera, M. Tandon, S. Pandey and K. K. Ghosh, Deep eutectic solvents as modulator on the micellization behavior of cationic surfactants and potential application in human serum albumin aggregation, *J. Mol. Liq.*, 2021, **344**, 117864.

32 M. K. Banjare, R. Kurrey, T. Yadav, S. Sinha, M. L. Satnami and K. K. Ghosh, A comparative study on the effect of 1-ethyl-3-methylimidazolium bromide on self-aggregation of aqueous cationic, anionic and non-ionic surfactants studied by surface tension, conductivity, fluorescence and FTIR Spectroscopy, *J. Mol. Liq.*, 2017, **241**, 622–632, DOI: **10.1016/j.molliq.2017.06.009**.

33 R. K. Banjare, M. K. Banjare, K. Behera, K. K Ghosh and S. Pandey, Micellization behaviour of conventional cationic surfactants within glycerol based deep eutectic solvent, *ACS Omega*, 2020, **31**, 19350–19362.

34 M. K. Banjare, K. Behera, R. Kumar Banjare, S. Pandey and K. K. Ghosh, Inclusion complexation of imidazolium-based ionic liquid and β-cyclodextrin : a detailed spectroscopic investigation, *J. Mol. Liq.*, 2020, **302**, 112530.

35 N. J. Turro and A. Yekta, Luminescent probes for detergent solutions. A simple procedure for determination of the mean aggregation number of micelles, *J. Am. Chem. Soc.*, 1978, **100**, 5951–5952.

36 M. K. Banjare, K. Behera, R. Kurre, R. K Banjare, M. L. Satnami, S. Pandey and K. K. Ghosh, Self-aggregation of bio-surfactants within ionic liquid 1-ethyl-3-methylimidazolium bromide: a comparative study and potential application in antidepressants drugs aggregation, *Spectrochim. Acta, Part A*, 2018, **199**, 376–386, DOI: **10.1016/j.saa.2018.03.079**.

37 M. K. Banjare, K. Behera, R. K. Banjare, S. Pandey and K. K. Ghosh, Multi-spectroscopic investigation on the inclusion complexation of β- cyclodextrin with long chain ionic liquid, *Carbohydr. Res.*, 2020, **491**, 107982.

38 S. Sharma, M. K. Banjare, N. Singh and K. K. Ghosh, Exploring spectroscopic insights into molecular recognition of potential anti-alzheimer's drugs within the hydrophobic pockets of β-cycloamylose, *J. Mol. Liq.*, 2020, **311**, 113269.

39 Komal, G. Singh, G. Singh and T. S. Kang, Aggregation behavior of sodium dioctyl sulfosuccinate in deep eutectic solvents and their mixtures with water: an account of solvent's polarity, cohesiveness, and solvent structure, *ACS Omega*, 2018, **3**, 13387–13398.

40 H. F. Mohd Zaid, C. F. Kait and M. I. A. Mutali, b Extractive deep desulfurization of diesel using choline chloride-glycerol eutectic-based ionic liquid as a green solvent, *Fuel*, 2017, **192**, 10–17.

41 H. Zhang, J. M. V. Luna, S. Tao, S. Calero, R. J. J. Riobóo, M. L. Ferrer, F. D. Monte and M. C. Gutiérrez, Transitioning from ionic liquids to deep eutectic solvents, *ACS Sustainable Chem. Eng.*, 2022, **10**(3), 1232–1245.

42 Y. He and X. Shen, Interaction between β-cyclodextrin and ionic liquids in aqueous solutions investigated by a competitive method using a substituted 3H-indole probe, *J. Photochem. Photobiol., A*, 2008, **197**, 253–259.

43 D. K. Mishra, G. Pugazhenthi and T. Banerjee, Ionic liquid-based deep eutectic solvent as reaction media for the thermal dehydrogenation of ethylene diamine-bis-borane, *ACS Sustainable Chem. Eng.*, 2020, **8**(12), 4910–4919.

44 H. Zhang, J. M. V. Luna, S. Tao, S. Calero, R. J. J. Riobóo, M. L. Ferrer, F. D. Monte and M. C. Gutiérrez, Transitioning from ionic liquids to deep eutectic solvents, *ACS Sustainable Chem. Eng.*, 2022, **10**(3), 1232–1245.

45 Y. Dai, J. V. Spronsen, G. J. Witkamp, R. Verpoorte and Y. H. Choi, Ionic liquids and deep eutectic solvents in natural products research: mixtures of solids as extraction solvents, *J. Nat. Prod.*, 2013, **76**(11), 2162–2173.